Chaotic stimulated Brillouin scattering in a finite-length medium

Carson C. Chow* and Abraham Bers
Plasma Fusion Center and Research Laboratory of Electronics, Massachusetts Institute of Technology, Cambridge, Massachusetts 02139
(Received 17 December 1992)

The dynamics of stimulated Brillouin scattering in a finite-length, homogeneous medium with the effects of temporal resonance detuning but no external feedback is examined numerically. The inclusion of resonance detuning leads to nonstationary behavior of the wave amplitudes including periodicity, quasiperiodicity, and chaos. The results may have applications to experiments with optical fibers and laser plasmas.

PACS number(s): 42.65.Es, 0.5.45.+b, 52.35.Nx

I. INTRODUCTION

The dynamics of stimulated Brillouin Scattering (SBS) in a homogeneous finite medium has captured considerable interest both in laser-plasma interactions [1–4] and in optical fibers [5–10]. SBS is a three-wave interaction (3WI) that results from a parametric coupling between electromagnetic (light) and acoustic waves. In an optical fiber, a laser impinges on the fiber, excites an acoustic wave by electrostriction, and scatters back (Stokes wave). In the case of a plasma an ion-acoustic wave is excited.

Nonstationary and chaotic behavior has been previously reported in SBS with external feedback such as reflection at the boundaries [1,2,4] or with models involving more than one pump [11,12]. Harrison *et al.* [9] have observed chaotic SBS experimentally in an optical fiber without feedback. Gaeta and Boyd [10] have performed similar experiments and obtained similar results. However, they propose that the experimentally observed aperiodic behavior is due to amplification of noise. They propose a stochastically driven model that agrees with their experiments.

It is shown here that with the addition of resonance detuning and without feedback the spatiotemporal 3WI modeling SBS can be chaotic in a restricted parameter regime. It has been demonstrated previously that unstable three wave interactions in time only (uniform amplitudes) with resonance detuning can have chaotic behavior provided the highest-frequency wave is unstable and the other two are damped [13,14]. The model we propose appears to be one of the simplest SBS models in spatially extended media that exhibits chaos; the highest frequency wave (the incident laser) is of course taken as stable.

The question remains as to how resonance detuning (i.e., frequency mismatch) would occur in a fiber. The experiments were done with narrow-linewidth lasers, so the resonance conditions should always be satisfied. An argument for how resonance detuning may arise has been proposed by Rubenchik [15]. The wavelength of the acoustic wave is on the order of the fiber diameter. Thus transverse modes will be set up in the fiber wave guide. The k spectrum will be discrete, so exact resonance may be impossible. Future experiments could seed the Stokes wave at a detuned frequency with a second laser, but at a low level so a three-wave interaction still applies.

For SBS in a finite medium with resonance detuning in one spatial dimension the equations are [16–18]

$$\partial_t a_i + v_i \partial_x a_i + \gamma_i a_i = -K a_j a_k \exp(-i\delta t), \tag{1a}$$

$$\partial_t a_j + v_j \partial_x a_j + \gamma_j a_j = K^* a_i a_k^* \exp(i\delta t), \tag{1b}$$

$$\partial_t a_k + v_k \partial_x a_k + \gamma_k a_k = K^* a_i a_j^* \exp(i\delta t), \tag{1c}$$

where power is fed in through the boundary with $a_i(0) = A_p$. Equations (1a) and (1b) describe the evolution of light waves traveling in opposite directions so $v_i = -v_j = c/n$, where c is the velocity of light and n is the index of refraction for the medium. Equation (1c) describes the evolution of the acoustic wave (ion acoustic wave in a plasma), where the group velocity is the sound velocity c_s. The resonance detuning parameter is δ. It should be noted that with fixed boundary conditions the resonance detuning cannot be transformed away in Eqs. (1a)–(1c).

In Eqs. (1a)–(1c), the slowly varying complex wave amplitudes a_n can be taken with units of electric field. Then, in a typical experiment with fused-silica optical fibers and a single-mode argon-ion laser operating at $\lambda =$ 514.5 nm, the parameters are $n = 1.46$, $c_s = 5.96 \times 10^3$ $\mathrm{m\,s^{-1}}$, $\gamma_k \simeq 270$ MHz, $K \simeq 66\ \mathrm{m\,s^{-1}\,V^{-1}}$, and $\gamma_i/\gamma_k \simeq 10^{-3}$ [5,9,10,19].

Equation (1) can be simplified. For a relatively strong pump the interaction time scale for the acoustic wave is given by $\tau = 1/(KA_p)$. This gives an interaction length of $l \simeq \tau\sqrt{c_s c/n}$. The damping length for the acoustic wave is $l_d \simeq c_s/\gamma_k$. For the case where the damping length is much smaller than the interaction length ($l_d \ll l$) the convective term in Eq. (1c) can be ignored. This condition is easily satisfied in optical fibers and can be satisfied in a plasma for heavy-ion acoustic-wave damping. The damping on the electromagnetic waves are weak and can be ignored. Length and time scales can be

rescaled with $\gamma_k t \rightarrow t$, $x\gamma_k(n/c) \rightarrow x$, $\Delta = \delta/\gamma_k$, and the wave amplitudes can be rescaled with $E_0 = a_i K/\gamma_k$, $E_s = a_j K/\gamma_k$, $E_a = (a_k K/\gamma_k)\exp(-i\Delta t)$. The SBS equations become

$$\partial_t E_0 + \partial_x E_0 = -E_s E_a, \tag{2a}$$

$$\partial_t E_s - \partial_x E_s = E_0 E_a^*, \tag{2b}$$

$$\partial_t E_a + (1 + i\Delta)E_a = E_0 E_s^*, \tag{2c}$$

with the boundary conditions $E_0(x = 0, t) = A_p K/\gamma_k \equiv A$, $E_s(x = L, t) = \epsilon$. The scattered wave is assumed to grow from a small amplitude (noise) ϵ at the right boundary. The laser wave E_0 is referred to as the pump, the scattered light wave E_s is often called the Stokes wave and E_a is the acoustic wave. In terms of a typical optical-fiber experiment, $L = 1$ corresponds to 0.75 m, $\Delta = 1$ corresponds to 270 MHz, and $A = \epsilon = 1$ corresponds to 4 MV m^{-1}.

II. THE DYNAMICS

Equations (2a)–(2c) were numerically simulated. The details of the numerical integration method are in Ref. [20]. For each run the spatiotemporal series was recorded. Diagnostics included monitoring the output time dependence of the waves: $E_0(x = L, t)$, $E_s(x = 0, t)$, $E_a(x = 0, t)$. The phase portrait of $E_a(0, t)$ vs $E_s(0, t)$ was constructed from this information. As a substitute for a Poincaré surface of section the phase portrait was strobed at the normalized detuning rate, i.e., $E_a(0, t_n)$ vs $E_s(0, t_n)$ where $t_n = 2\pi n/\Delta$, n is an integer. The system has four free parameters A, Δ, ϵ, and L. However, a numerical survey of the parameter space indicated that a two-dimensional surface in the parameter space could capture the unfolding behavior. The Δ-A parameter plane for fixed L and ϵ was chosen.

Figure 1 shows the numerically determined unfolding diagram in the Δ-A plane for $L = 40$ and $\epsilon = 0.0025$. Parameters L and ϵ were chosen so that the bifurcation diagram in the Δ-A plane contained all the observed dynamics. For small Δ and A there is a stable fixed state. It becomes unstable through a Hopf bifurcation to a periodic state. Then there is a transition to quasiperiodicity and to chaos. Each region will be discussed in detail.

A. The fixed state

The system has one fixed state. This is best examined by transforming the complex amplitudes to modulus-phase form. Substituting the following:

$$E_0 = A_0 e^{i\phi_0}, \tag{3a}$$

$$E_s = A_s e^{i\phi_s}, \tag{3b}$$

$$E_a = A_a e^{i\phi_a}, \tag{3c}$$

into Eqs. (2a)–(2c) yields the equations

$$A_{0,t} + A_{0,x} = -A_s A_a \cos\phi, \tag{4a}$$

$$A_{s,t} - A_{s,x} = A_0 A_a \cos\phi, \tag{4b}$$

$$A_{a,t} + A_a = A_0 A_s \cos\phi, \tag{4c}$$

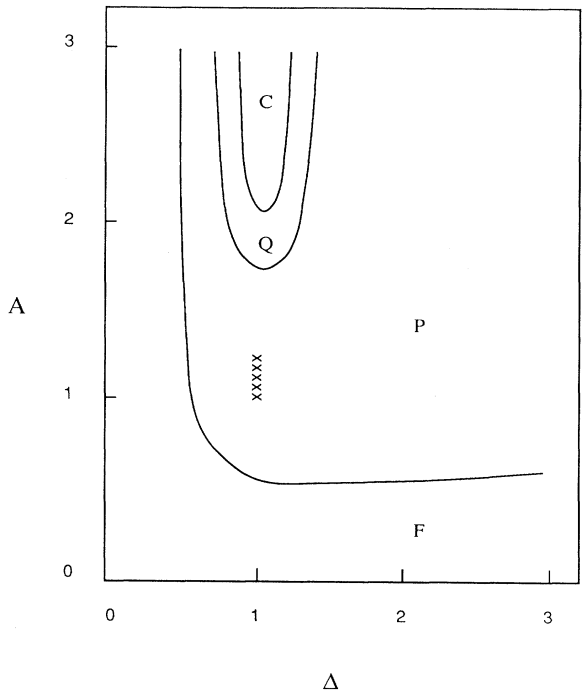

FIG. 1. Bifurcation diagram in the Δ-A plane for $L = 40$ and $\epsilon = 0.0025$. There are four different phases: F denotes the fixed state, P denotes the periodic orbit, Q denotes quasiperiodicity, and C denotes chaos. The line of $\times$'s indicates a region of phase coexistence between a periodic and a quasiperiodic orbit.

$$\phi_{0,t} + \phi_{0,x} = -\frac{A_s A_a}{A_0}\sin\phi, \tag{5a}$$

$$\phi_{s,t} - \phi_{s,x} = -\frac{A_0 A_a}{A_s}\sin\phi, \tag{5b}$$

$$\phi_{a,t} + \Delta = -\frac{A_0 A_s}{A_a}\sin\phi, \tag{5c}$$

where $\phi = \phi_a + \phi_s - \phi_0$. The fixed state is obtained by setting the time derivatives to zero. From Eqs. (4a)–(4c) this yields the equations

$$A_{0,x} = -A_0 A_s^2 \cos^2\phi, \tag{6}$$

$$A_{s,x} = -A_0^2 A_s \cos^2\phi. \tag{7}$$

Combining Eqs. (4c) and (5c) yields $\tan\phi = -\Delta$. The amplitudes must be positive so from (4c) it can be concluded that

$$\cos\phi = \frac{1}{\sqrt{1+\Delta^2}}, \quad \sin\phi = \frac{-\Delta}{\sqrt{1+\Delta^2}}. \tag{8}$$

Equations (6) and (7) can then be integrated to yield

$$A_0^2 = \frac{A^2(1-R)}{1 - R\exp[-2(1-R)A^2\Gamma x]}, \tag{9a}$$

$$A_s^2 = \frac{A^2 R(1-R)}{\exp[2(1-R)A^2\Gamma x] - R}, \tag{9b}$$

$$A_a = \Gamma^{1/2} A_0 A_s, \quad \Gamma = (1+\Delta^2)^{-1}, \tag{9c}$$

subject to

$$A_s(x = L) = \epsilon. \tag{10}$$

The reflectivity R is determined by the boundary condition at $x = L$. Its value must be obtained numerically.

Substituting for A_a and $\sin\phi$ in Eqs. (5b) and (5c) yields

$$\phi_{0,x} = \frac{\Delta}{1+\Delta^2} A_s^2, \tag{11}$$

$$\phi_{s,x} = -\frac{\Delta}{1+\Delta^2} A_0^2. \tag{12}$$

Using Eqs. (9a) and (9b), the phases in Eqs. (11) and (12) can be integrated to yield

$$\phi_0 = \frac{\Delta}{2} \ln\left[\frac{1 - R\exp[-2A^2(1-R)\Gamma x]}{1-R}\right], \tag{13}$$

$$\phi_s = -\frac{\Delta}{2} \ln\left[\frac{\exp[2A^2(1-R)\Gamma x] - R}{\exp[2A^2(1-R)\Gamma L] - R}\right], \tag{14}$$

where the boundary conditions

$$\phi_0(x = 0) = 0, \quad \phi_s(x = L) = 0 \tag{15}$$

have been applied. The phases are fixed by the boundary conditions and increase as they travel towards the opposite end. The pump phase has an upper bound of $\phi_0(L) \leq -(\Delta/2)\ln(1-R)$ while the Stokes phase is unbounded for large A.

The spatial profile of the fixed state for the envelope moduli for parameters $A = 1.6$, $\Delta = 0$, $L = 40$, and $\epsilon = 0.0025$ is shown in Fig. 2. In this particular example the reflectivity R for the Stokes wave is close to unity. The Stokes wave has a definite decay length in space given by

$$l_s \simeq (1+\Delta^2)/[2(1-R)A^2]. \tag{16}$$

For distances beyond $x \simeq l_s$ the Stokes wave has negligible amplitude and the pump no longer couples to the other two waves. Thus l_s gives an effective interaction length. Although the system box may be larger, the dynamics take place in the interaction region $0 < x < l_s$.

The stability of the fixed state can be examined by substituting $E_l = A_l \exp(i\phi_l) + \delta E_l$ into Eqs. (2a)–(2c), where δE_l are small perturbations. If the perturbations are assumed to have a time dependence of $\exp(st)$, the linearized equations form an inhomogeneous fourth-order boundary-value problem for the real and imaginary parts of δE_0 and δE_s. These equations must be solved numerically. This has not yet been done. For no resonance detuning ($\Delta = 0$), Blaha *et al.* [3] showed that this fourth-order system reduces to two second-order equations, one each for the real and imaginary parts. These second-order equations can then each be transformed into Legendre equations and the time evolution of perturbations can be found in terms of associated Legendre functions. They showed that the fixed state is unstable in a semi-infinite medium. Applying boundary conditions for a finite medium to their solutions, the fixed state can be shown to always be stable for no resonance detuning.

Numerically it was found that the fixed-state Hopf bifurcates to a periodic state along an L-shaped curve in the parameter plane (see Fig. 1). Although an analytic condition for the stability of the fixed state has not been found, this particular shape can be understood qualitatively. Consider a nonzero value of A. The fixed state is stable for $\Delta = 0$. The only difference in the fixed state between $\Delta = 0$ and $\Delta \neq 0$ is the "phase twist" given in Eqs. (13) and (14). The criterion for stability is then postulated to be determined by the amount of "phase twisting." For example, when $\phi_s(x = 0)$ exceeds a critical threshold, the fixed state becomes unstable. A contour portrait of $\phi_s(x = 0)$ in the Δ-A plane for $L = 40$ and $\epsilon = 0.0025$ is shown in Fig. 3. Notice that the $\phi_s(x = 0) \simeq 5$ contour matches very closely to the numerically determined stability boundary in Fig. 1.

From Eq. (14) it appears that the phase $\phi_s(0)$ depends on A^2 and L in the same way. This is not entirely true because the reflection coefficient depends nontrivially on

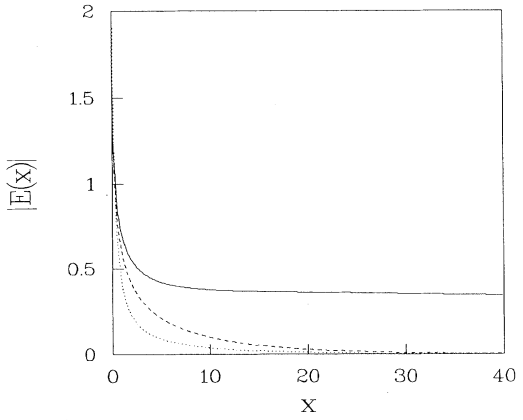

FIG. 2. Fixed-state spatial profiles of the pump (solid line), Stokes wave (dashed line), and acoustic wave (dotted line) for the parameters $\Delta = 0$, $A = 1.6$, $L = 20$, and $\epsilon = 0.0025$.

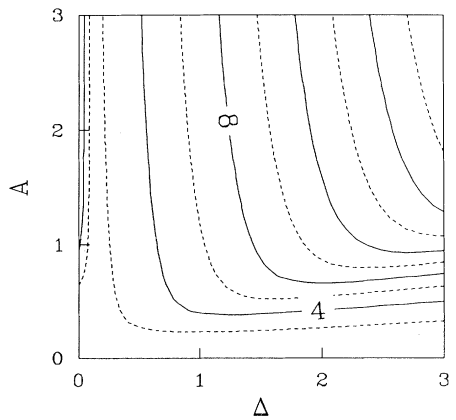

FIG. 3. Contour plot of $\phi_s(x = 0)$ in the Δ-A plane for $L = 40$, and $\epsilon = 0.0025$.

the parameters. However, it has a relatively weak dependence and numerical simulations do show that the bifurcation point responds similarly to A^2 and L. In the parameter plane (Fig. 1), L was set large enough so that all the bifurcations were included.

B. Periodic orbits

When the stability line is crossed in parameter space the fixed-state Hopf bifurcates to a periodic state. Points in the parameter plane will be denoted by the ordered pair (Δ, A). An example of the spatial profile of a periodic state at $(1,1)$ is shown in Fig. 4. The three profiles have the form of the fixed-state profiles shown in Fig. 2, but with modulations. In this and the following spatial profile figures, the pump is the solid line, the Stokes wave is the dashed line, and the acoustic wave is the dotted line. The pump consists of a periodic pattern that propagates across the box. The interaction between the waves is confined to a small region given roughly by the decay length of the Stokes wave Eq. (16). The time series of the output pump amplitude will be identical to the spatial profile of the pump outside of the interaction region with the other two waves. The output time series of the pump and Stokes waves are both periodic. The power spectrum of the pump is shown in Fig. 5 and shows the frequency is very near Δ. The power spectra of the other two waves are similar. The phase portrait of E_s vs E_a is shown in Fig. 6(a). A closed curve is seen confirming periodic behavior. The phase portrait strobed at the normalized detuning rate $\Delta = 1$ is shown in Fig. 6(b). In this case the frequency is locked to the detuning rate with a period of 38. In all cases the frequency will be near Δ, but not necessarily locked to it.

One small section of the periodic regime, indicated by a line of crosses in Fig. 1, has a phase coexistence between a periodic state and a quasiperiodic state. Depending on the initial conditions, the result could be a periodic state similar to that seen in Fig. 6 or a completely different quasiperiodic orbit can appear. Figure 7 shows the phase portrait of the quasiperiodic state. One sees

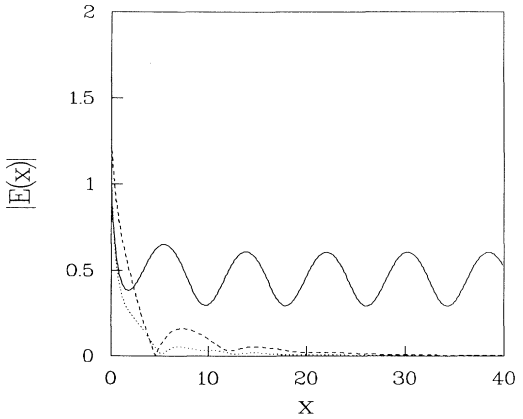

FIG. 4. Periodic state: spatial profile of the amplitudes at a fixed time at (1,1).

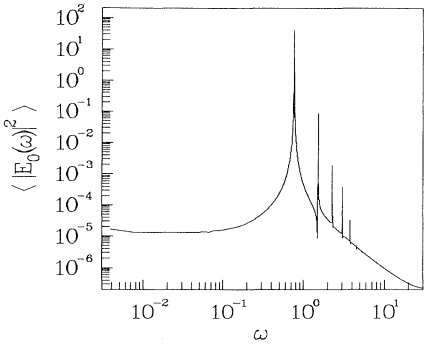

FIG. 5. Periodic state: power spectrum of pump at (1,1).

a double-looped figure that does not close. The two different runs were continued for very long times to test their robustness. However, even after many hundreds of thousands of periods, the quasiperiodic state did not fall into the periodic attractor. It is unknown what the basin of attraction is for each phase. This coexistence regime was discovered by chance. It is unknown whether more regimes exist in the periodic regime. In many of the runs

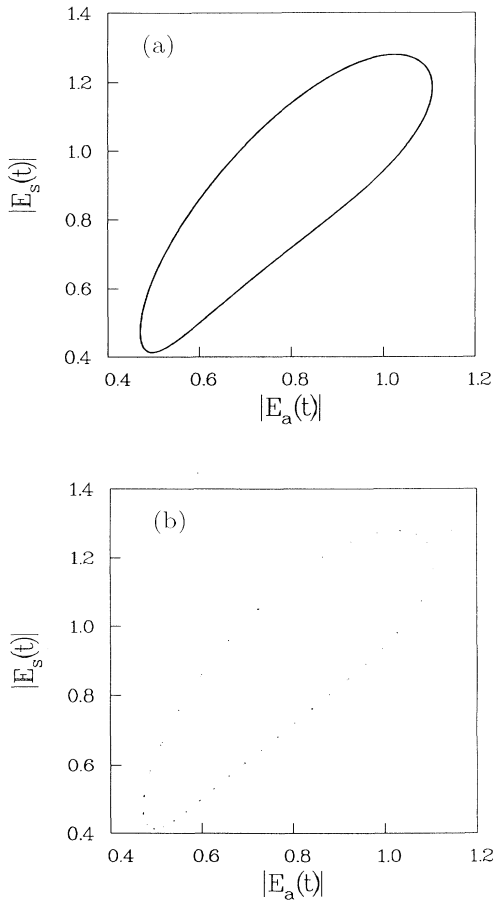

FIG. 6. Periodic state: (a) phase portrait E_s vs E_a at (1,1); (b) phase portrait strobed at $t_n = 2\pi/\Delta$.

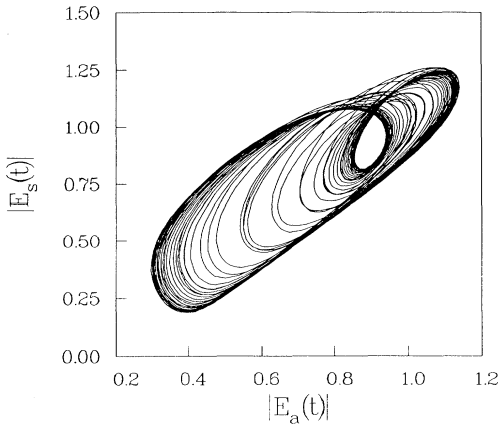

FIG. 7. Quasiperiodic state: phase portrait at (1.1,1). This state coexists with a periodic state.

made in the periodic regime, the relaxation times were extremely long. Often it was difficult to distinguish between periodic and nonperiodic states because the transients were so long lived.

C. Quasiperiodicity and chaos

By changing the parameters the periodic state can make a transition to a quasiperiodic state. As the bifurcation boundary to quasiperiodicity is approached from the periodic side, a second frequency corresponding to the round-trip transit time across the box begins to make an appearance as a transient oscillation. Its decay time becomes longer and longer as the boundary is approached until it no longer decays away at the boundary between periodicity and quasiperiodicity. Very long computation times were required to resolve this boundary.

The power spectrum for the pump for the quasiperiodic state at $(1,2)$ is in Fig. 8. The other waves have similar power spectra. There are many peaks in the spectrum confirming quasiperiodic behavior. The peak at $\omega \simeq 1$ is the fast frequency from the periodic orbit. The broader peak near $\omega \simeq 0.07$ corresponds to a time scale of twice the transit time across the box. The phase

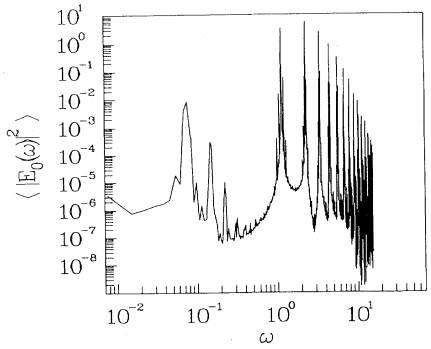

FIG. 8. Quasiperiodic state: power spectrum of the pump at (1,2).

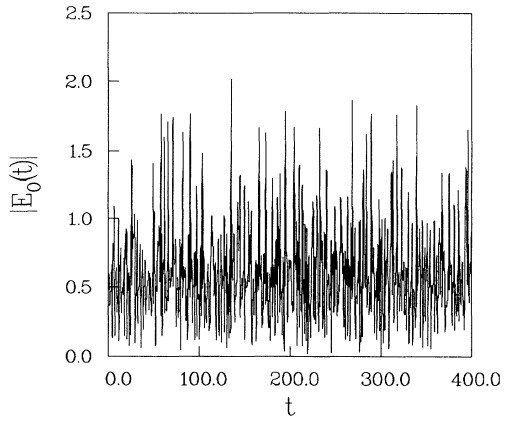

FIG. 9. Chaotic state: time series of pump at (1,5).

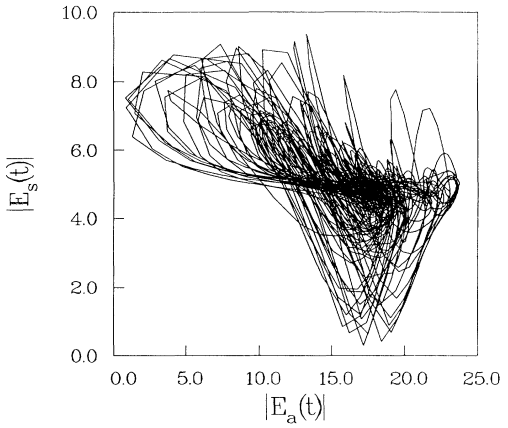

FIG. 10. Chaotic state: phase portrait at (1,5).

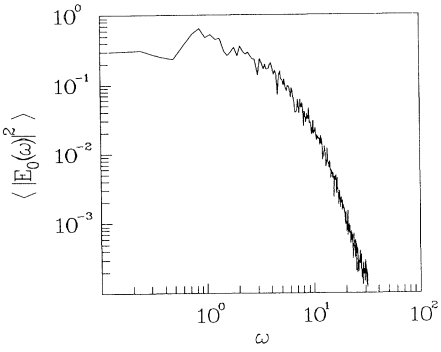

FIG. 11. Chaotic state: power spectrum of the pump at (1,5).

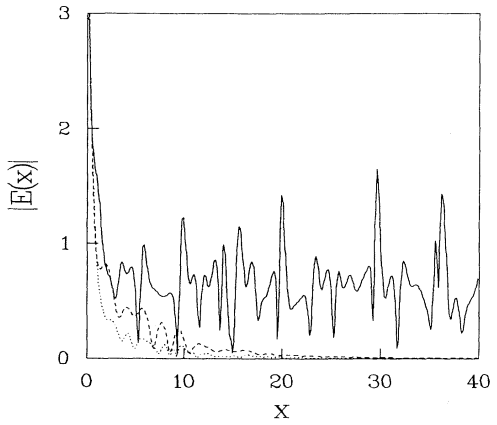

FIG. 12. Chaotic state: spatial profile at (1,5).

portrait will have a width and be clearly nonperiodic.

The quasiperiodic state makes a subcritical bifurcation to chaos. At the boundary between the two phases there is a region of hysteresis. However, this region is very narrow. For instance at $(1,2)$ there is another attractor. The phase portrait shows that the orbit has a double-loop structure similar to that for the quasiperiodic phase at $(1.1,1)$ seen in Fig. 7. The orbit alternates between one loop and the other. The output time series seem to manifest intermittency. The time-only equations were observed to exhibit type-I intermittency [14]. The power spectrum for the pump shows broadband behavior indicative of chaos. A measurement of the largest Lyapunov exponent λ was made by linearizing about a fiducial orbit (see Ref. [21]). It was found to be very small but positive ($\lambda \simeq 0.001$).

As the chaotic regime is entered further the orbits become more aperiodic. The laminar regions in the time series reduce in size and the general structure of the time series begins to look different. A third loop in the phase portrait begins to form. Well into the chaotic region at (1,5), the time series of the pump is clearly chaotic in Fig. 9. The phase portrait in Fig. 10 has no real structure. The power spectrum in Fig. 11 flattens out below $\omega \simeq 1$, defining a coherence or correlation time where the spectrum bends over. The spatial profile is in Fig. 12. The waves appear chaotic yet the interaction length where the Stokes wave has substantial amplitude remains small. From the plot it appears that the coherence length of the pump structures is on the order of the decay length of the Stokes wave. Thus the resulting chaos is expected to be low dimensional.

III. CONCLUSIONS

Given that resonance detuning is present in SBS, a sequence of transitions from steady state to chaos is possible. For the chaotic regime to occur, the reflectivity must be high and the medium must be larger than the decay length (growth length) for the Stokes wave. The parameter unfolding of the system is complicated and difficult to understand. Even the linear stability analysis is unwieldy. However the phase-twist hypothesis for instability of the fixed state seems to capture the behaviour qualitatively. This fact, along with the existence of a relatively well-defined bifurcation sequence to chaos, is an indication that there may be a reduced ordinary-differential-equation description for the dynamics. This is in contrast to other models of nonlinear three wave interactions where spatiotemporal chaos with many degrees of freedom is observed [22]. The difficulty of the model considered here is that the boundary conditions impose an inhomogeneous fixed state. The linear equations must be solved numerically to obtain the eigenvalues. Simple expansions in a harmonic series do not satisfy the boundary conditions. Thus, some nontrivial mode expansion is likely to be required.

The addition of resonance detuning appears to provide the simplest SBS model thus far that has chaotic solutions. Gaeta and Boyd [10] have strong evidence that the aperiodicity observed thus far in experiments with optical fibers is due to amplification of noise. This is not to say that chaotic SBS due to resonance detuning may not exist in other experiments. For high reflectivity in a large medium the effect of the noise need not be as great [23]. Future experiments using a second laser at very low powers to seed the Stokes wave may be employed to reduce the effects of noise. The temperature of the optical fiber could also be lowered to reduce the noise. The frequencies could be scanned to search for acoustic modes that would lead to dephased SBS. The power of the lasers and length of the fiber could then be varied to search for chaotic behavior.

ACKNOWLEDGMENTS

We wish to thank H. Haus and A. Gaeta for very interesting and informative discussions. This research was supported in part by National Science Foundation Grant No. ECS-88-2475 and Lawrence Livermore National Laboratory subcontract No. B160456.

* Present address: Department of Astrophysical, Planetary and Atmospheric Sciences, University of Colorado, Boulder, CO 80309.

[1] C.J. Randall and J.R. Albritton, Phys. Rev. Lett. **52**, 1887 (1984).
[2] K. Sauer and K. Baumgärtel, Phys. Rev. Lett. **52**, 101 (1984).
[3] R. Blaha, E.W. Laedke, A.M. Rubenchik, and K.H. Spatschek, Europhys. Lett. **7**, 237 (1988).
[4] S. Hüller, P. Mulser, and A.M. Rubenchik, Phys. Fluids B **3**, 3339 (1991).
[5] D. Cotter, J. Opt. Commun. **4**, 10 (1983).

[6] I. Bar-Joseph, A.A. Friesem, E. Lichtman, and R.G. Waarts, J. Opt. Soc. Am. B **2**, 1606 (1985).
[7] J. Coste and C. Montes, Phys. Rev. A **34**, 3940 (1986).
[8] J. Botineau, C. Leycuras, C. Montes, and E. Picholle, J. Opt. Soc. Am. B **6**, 300 (1989).
[9] R.G. Harrison, J.S. Uppal, A. Johnstone, and J.V. Moloney, Phys. Rev. Lett. **65**, 167 (1990).
[10] A.L. Gaeta and R.W. Boyd, Phys. Rev. A **44**, 3205 (1991).
[11] P. Narum, A.L. Gaeta, M.D. Skeldon, and R.W. Boyd, J. Opt. Soc. Am. B **5**, 623 (1988).
[12] A.L. Gaeta, M.D. Skeldon, R.W. Boyd, and P. Narum, J. Opt. Soc. Am. B **6**, 1709 (1989).
[13] J. Wersinger, J. Finn, and E. Ott, Phys. Fluids **23**, 1142 (1980).
[14] C. Meunier, M. Bussac, and G. Laval, Physica **4D**, 236 (1982).
[15] A.M. Rubenchick (private communication).
[16] N.M. Kroll, Proc. IEEE **51**, 110 (1963).
[17] N. Bloembergen, *Nonlinear Optics* (Benjamin, New York, 1965).
[18] W. Kaiser and M. Maier, in *Laser Handbook, Vol. 2*, edited by F.T. Arecchi and S. Dubois (North-Holland, Amsterdam, 1979).
[19] D. Cotter, Opt. Quantum Electron. **19**, 1 (1987).
[20] C.C. Chow, Ph.D. thesis, Massachusetts Institute of Technology, 1992 (unpublished).
[21] A. Wolf, J.B. Swift, H.L. Swinney, and J.A. Vastano, Physica **16D**, 285 (1985).
[22] C.C. Chow, A. Bers, and A.K. Ram, Phys. Rev. Lett. **68**, 3379 (1992).
[23] A.L. Gaeta (private communication).